

Fabrication and performance of blazed transmission gratings for x-ray astronomy

Ralf K. Heilmann, Minseung Ahn, and Mark L. Schattenburg

Space Nanotechnology Laboratory, MIT Kavli Institute for Astrophysics and Space Research,
Massachusetts Institute of Technology,
77 Massachusetts Avenue, Cambridge, Massachusetts 02139, USA

ABSTRACT

We have developed a new type of soft x-ray diffraction grating. This critical-angle transmission (CAT) grating combines the advantages of traditional transmission gratings (low mass, extremely relaxed alignment and flatness tolerances) with those of x-ray reflection gratings (high efficiency due to blazing in the direction of grazing-incidence reflection, increased resolution due to the use of higher diffraction orders). In addition, grating spectrometers based on CAT gratings are well-suited for co-existence with high-energy focal plane microcalorimeter detectors as planned for the Constellation-X mission, since most high-energy x rays are neither absorbed nor deflected, and arrive at the telescope focus. We describe the CAT grating principle and design, and fabrication and x-ray diffraction efficiency results for a CAT grating with 1742 lines/mm. We have observed up to 46% diffraction efficiency in a single order, and up to 55% at blaze at extreme ultraviolet wavelengths. We present our recent fabrication and soft x-ray diffraction results for 200 nm-period (5000 lines/mm) gratings.

Keywords: x-ray optics, Constellation-X, critical-angle transmission grating, x-ray spectroscopy, blazed transmission grating, extreme ultraviolet, soft x-ray

1. INTRODUCTION

X-ray spectroscopy provides invaluable quantitative data in the field of high-energy astrophysics.¹ The wavelengths of interest extend over several orders of magnitude, so it is not surprising that a single spectrometer can not cover such a large range with the highest resolution. Current designs for Constellation-X, NASA's next-generation x-ray observatory, need to provide large collecting area and high spectral resolution over the 0.3 to 40 keV photon energy range (~ 0.03 to 4.1 nm wavelengths). An x-ray microcalorimeter detector at the telescope focus provides fixed energy resolution of $\Delta E \sim 2.5$ eV, resulting in $E/\Delta E \sim 2400$ at 6 keV. However, at low energies $E/\Delta E$ becomes small and wavelength dispersive diffraction gratings offer superior resolution. For that reason an x-ray grating spectrometer is expected to disperse a fraction of the incident low energy photon flux (0.3 - 1 keV) away from the telescope focus onto a separate CCD detector array.

Grating-based x-ray spectroscopy in space has a successful heritage. In the past two separate mounting geometries have been realized. On Einstein,² EXOSAT,³ and Chandra⁴ transmission gratings were implemented, while XMM-Newton employs in-plane reflection gratings.⁵ With the excellent 0.5 arcsec angular resolution of the Chandra mirrors the High-Energy Transmission Grating Spectrometer (HETGS) achieves spectral resolution up to 1500 in first order, albeit with very small effective area. The Constellation-X telescope mirrors will provide much larger collecting area, but due to their segmented geometry and thin-foil-like dimensions the mirror assembly angular resolution goal is only 5 arcsec. This makes it difficult to achieve high spectral resolution with a traditional 200 nm-period transmission grating in first order, which was the state of the art in the early 1990's. The same argument applies to XMM-Newton (mirrors with 14 arcsec half energy width (HEW)). To achieve the high dispersion required to compensate for the broad telescope point-spread-function (PSF) for XMM-Newton an in-plane grazing incidence reflection grating spectrometer (RGS) was built that provides $E/\Delta E$ up to 500. While the in-plane geometry produces high dispersion with easy-to-fabricate large-period gratings, its diffraction efficiency peaks below 30% despite blazing.^{6,7} Higher diffraction efficiency around 70% is predicted for blazed

Further author information: Send correspondence to R.K.H. E-mail: ralf@space.mit.edu, URL: <http://snl.mit.edu/>

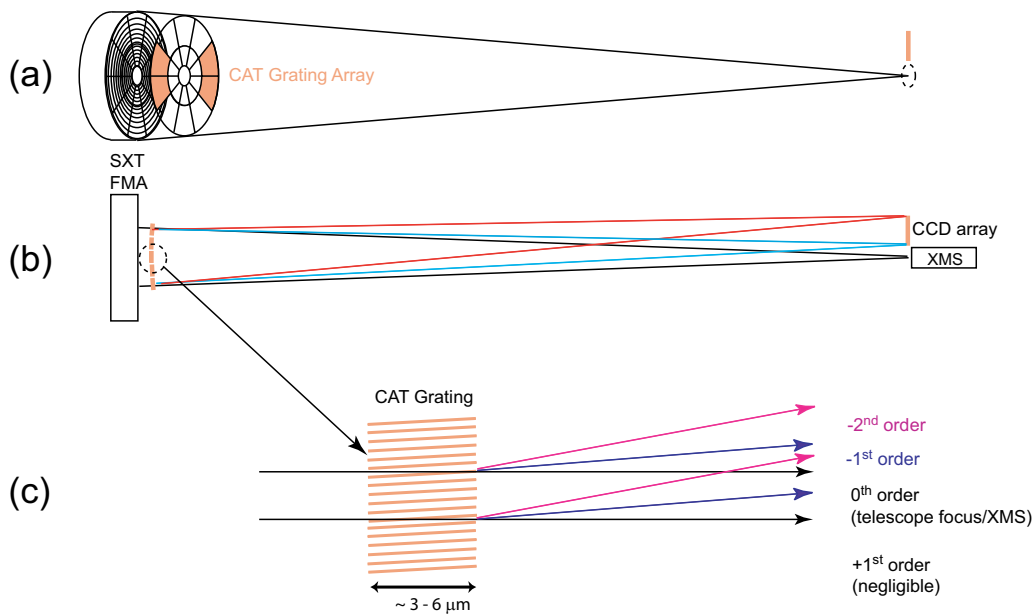


Figure 1. Schematic of CAT grating spectrometer. (a) Perspective view. The grating array is removed from the Spectroscopy X-ray Telescope (SXT) Flight Mirror Assembly (FMA) for a better view. The lightweight array can be mounted to the downstream end of the FMA. The two 72° segments disperse soft x-rays onto a single CCD array offset from the X-ray Microcalorimeter Spectrograph (XMS) at the telescope focus. The CCDs only need to capture the angular range that corresponds to the blaze envelope. (b) Side view, showing shorter wavelength or lower diffraction order lines focusing closer to the optical axis. (c) Blow-up, showing a cross section through a CAT grating, and the directions of a few diffraction orders. (The signs of the diffraction orders have no physical significance and depend on choice of definitions.)

grazing-incidence reflection gratings in the extreme off-plane mount,⁸ and up to 40% efficiency in a single order has been demonstrated.^{7,9-12} The off-plane grating can be blazed for higher diffraction orders, which helps to increase spectral resolution,¹³ but requires the same small grating periods as a transmission grating. Both types of grazing-incidence reflection gratings must fulfill stringent surface figure and alignment requirements¹⁴ to avoid degradation of the telescope PSF and loss of spectral resolution, which of course is more difficult to achieve for high-resolution telescopes with a small PSF. Competing with challenging figure requirements is the demand for low weight and minimal obscuration, driving reflection grating substrates into the same thin-foil optic realm (densely stacked, $400 \mu\text{m}$ thin, $100 \times 200 \text{ mm}^2$ foils) as the telescope mirrors themselves.

Normal incidence transmission gratings, on the other hand, provide diffracted beams that are orders of magnitude less sensitive than reflected diffraction orders to non-ideal grating figure or misalignment for typical soft x-ray parameters.¹⁵ As a further advantage they only need to be a few μm thick, which makes them much lighter than grazing incidence reflection gratings. However, traditional phase-shifting transmission gratings suffer from low diffraction efficiency in the soft x-ray band due to absorption upon transmission through the grating material.

We have recently developed a new transmission grating design that combines the advantages of reflection gratings and transmission gratings.¹⁵ In the following we will describe its features and operating principles, fabrication and x-ray tests of a first prototype with a period of 574 nm (1742 lines/mm), and the current fabrication status of 200 nm -period gratings. We will also present some raw data from the first x-ray diffraction measurements of those 200 nm -period critical-angle transmission gratings.

2. THE CRITICAL-ANGLE TRANSMISSION (CAT) GRATING

2.1 The Basic Idea

The soft x-ray band contains a wealth of characteristic lines and, accordingly, photons experience relatively short absorption lengths in matter.¹⁶ A transmission grating with high efficiency over a broad band should therefore minimize the amount of material to be traversed, while at the same time shifting energy from the dispersionless 0th order straight-through path into (ideally) one desired non-zero diffraction order. This requires a change in direction of the photon wave vector. Semantics aside there are three basic means to divert x rays efficiently. The first two are phase-shifting and diffraction, both of which are strongly wavelength-dependent, and the third is through specular reflection at grazing angles of incidence below the critical angle for total external reflection. The latter two are used in blazed reflection gratings, where diffraction efficiency for diffraction orders in the direction of specular reflection from a grating facet is enhanced. The same broadband blazing effect can be achieved in transmission geometry, as we explain in the following.

A CAT grating consists of free-standing grating bars that are only supported on their sides by a coarse support mesh. Photons are incident onto the grating bar sidewalls at some angle α below the critical angle for total external reflection, θ_c (see Fig. 2). In this design the grating bar sidewalls serve as blaze facets. In order for every photon incident upon a gap between grating bars to undergo a single reflection the grating depth d should be $d = a/\tan\alpha$, with a being the space between two neighboring grating bars. At the same time the grating bar thickness b should be as small as possible to minimize absorption or blockage of x rays. The grating bar sidewalls must be smooth enough to prevent scattering losses. For soft x rays θ_c is typically on the order of $1 - 5^\circ$.

The grating equation gives the angles β_m at which the m^{th} diffracted order is observed when a wave of wavelength λ is incident onto a periodic structure with period p at an angle α . The angles are defined relative to the normal to the direction of periodicity:

$$\frac{m\lambda}{p} = \sin\alpha - \sin\beta_m, \quad (1)$$

with $m = 0, \pm 1, \pm 2, \dots$. In order for β_m to be reasonably small for small m and for soft x rays the grating period needs to be on the order of a few hundred nm or less. A set of parameters that describes one possible design for a CAT grating-based transmission grating spectrometer that fulfills all Constellation-X requirements is $p = 100$ nm, $b = 20$ nm, $\alpha = 1.5^\circ$, which leads to $d = 3055$ nm, and a high aspect ratio of $d/b \approx 150$ for the grating bars. If the grating bar sidewall microroughness is below ~ 1 nm the walls act as efficient silicon mirrors.

While the grating equation easily tells the directions of the diffracted orders it says nothing about the distribution of diffracted intensity in the different orders. A simple, physically intuitive model for the diffraction efficiency of CAT gratings was given in Ref. 15 and is briefly summarized here. In the Fraunhofer approximation of scalar Kirchhoff diffraction theory the diffraction efficiency of a grating can be written as the product of two factors.¹⁷ For an infinite grating the first factor is a set of delta functions at angles identical to the grating equation. The second factor is the intensity distribution for diffraction from a single grating element of dimension p . Assuming that $\alpha = \tan^{-1}(d/a)$, we describe the diffraction from a single CAT grating slot in the direction of some angle β relative to the silicon mirror surface simply as a specular reflection, which changes the sign of β , immediately followed by diffraction from a slit of width a . We then scale the efficiency by the specular reflectivity of silicon $R(\alpha, \lambda)$ and multiply by a/p , assuming that all photons hitting the top of a grating bar (width $b = p - a$) are absorbed. The result can be written as

$$I(\lambda, p, \alpha, \beta, k, a, R) = I_{\text{grat}} I_{\text{slit}} R(\alpha, \lambda) (a/p), \quad (2)$$

where

$$I_{\text{grat}}(\lambda, p, \alpha, \beta, k) = \left| \frac{\sin kg}{k \sin g} \right|^2, \quad (3)$$

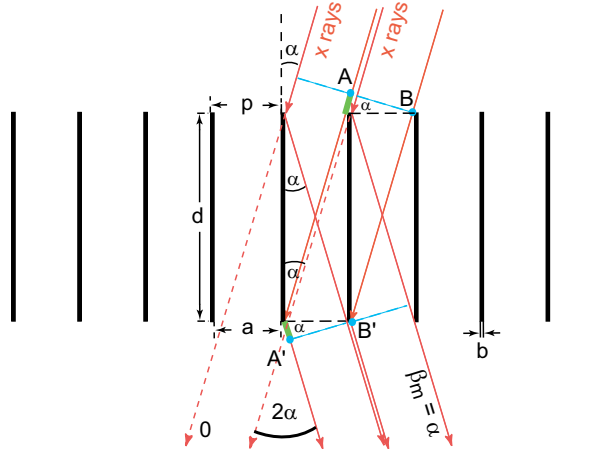


Figure 2. Schematic of a cross section through a CAT grating. The m^{th} diffraction order occurs at an angle β_m where the path length difference between AA' and BB' is $m\lambda$. Shown is the case where β_m coincides with the direction of specular reflection from the grating bar sidewalls ($\beta_m = \alpha$), i.e. blazing in the m^{th} order.

and

$$I_{\text{slit}}(\lambda, \alpha, \beta, a) = \left| \frac{\sin f}{f} \right|^2. \quad (4)$$

The functions g and f are defined as $g = p(\pi/\lambda)(\sin \beta - \sin \alpha)$, and $f = a(\pi/\lambda)(-\sin \beta - \sin \alpha)$, and k is the number of grating elements. The single slit diffraction defines a blaze envelope with a width inversely proportional to the slit width a that modulates the intensity of the diffraction orders. Rotating the grating relative to an incident beam by an angle γ shifts the blaze envelope by 2γ in the laboratory frame defined by the incident beam. However, the transmitted diffraction orders themselves only shift by amounts $(\gamma/2)(m\lambda/p)^2$ relative to the incident beam - three to four orders of magnitude less than reflected orders. This shift is described by Eq. (3) alone, and it is independent from the details of the individual grating element.

A more accurate estimate of the diffraction efficiency can be obtained through the so-called rigorous coupled-wave analysis (RCWA).¹⁸ Predictions for the above model CAT grating are shown in Fig. 3. Longer wavelengths are blazed in first order. Towards shorter wavelengths higher orders move into and out of the blaze envelope, until the fixed angle of incidence exceeds $\theta_c(\lambda)$ at short enough wavelengths. At these higher photon energies the silicon mirrors become increasingly transparent, and the CAT grating turns into a very ineffective phase grating with most of the photons transmitted in 0^{th} order. In the case of Constellation-X this means that high energy x rays are not lost, but instead proceed without deviation to the telescope focus and contribute to the microcalorimeter effective area. This is in contrast to reflection gratings, which block x rays of any energy from reaching the calorimeter. CAT gratings also display very high broadband diffraction efficiency close to the mirror reflectivity times a/p , and with theoretical values very similar to theoretical predictions for off-plane reflection gratings.

2.2 Spectral Resolution and Sub-Aperturing

The spectral resolution $E/\Delta E$ or $\lambda/\Delta\lambda$ for a grating placed into the converging beam of an x-ray telescope is usually dominated by the PSF of the telescope. A simple resolution estimate is given by looking at how different two wavelengths have to be in order to be separated by an amount equal to the PSF in the dispersed spectrum. For a CAT grating the diffraction intensities will be concentrated around the peak of the blaze envelope, which in our case is at $2 \times 1.5^\circ = 3.0^\circ$ from the incident beam. If the grating is mounted at the back of the mirror assembly its distance to the focal plane is close to the focal length of the slow telescope, and we obtain a resolution of $\sim 3^\circ/15 \text{ arcsec} = 720$ for a telescope with a 15 arcsec angular PSF. At some wavelengths two orders will contribute significantly to the diffraction efficiency, with the higher order having higher spectral

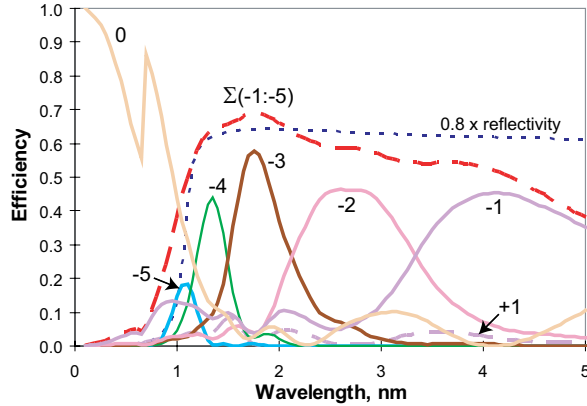


Figure 3. RCWA diffraction efficiency predictions for a silicon CAT grating with $p = 100$ nm, $d = 3055$ nm, $b = 20$ nm, and $\alpha = 1.5^\circ$. The specular reflectivity for silicon, multiplied by $a/p = 0.8$, is also shown for comparison. Blazing is evident, as the +1 order (dashed line at the bottom) is much weaker than the -1 order. The sum of blazed diffraction orders (upper dashed line) is between 50 and 70% over a broad range of wavelengths. At shorter wavelengths ($\theta_c(\lambda) < \alpha$) the CAT grating becomes increasingly transparent, and the strong 0^{th} order is transmitted to the telescope focus with very little attenuation.

resolution and the lower order having lower resolution. Weighting the resolution for each wavelength by the relative efficiencies of its blazed orders leads to an average spectral resolution close to the same value as above.¹⁹

The spectral resolution can be increased through sub-aperturing, i.e. by limiting the mirror coverage by gratings in the azimuthal direction to two opposing 72° segments. Ray traces predict spectral resolution > 1700 (half energy width) over the 1-5 nm band in this case.¹⁹ For a 5 arcsec telescope optic the resolution is expected to become greater than 4000.¹⁹

3. FABRICATION OF CAT GRATING PROTOTYPES

The geometrical requirements for CAT gratings as outlined above are challenging to realize. We developed a fabrication process that uses a $\langle 110 \rangle$ silicon-on-insulator (SOI) wafer as a starting point with a device layer thickness equal to the desired grating thickness d .²⁰ The four main process steps are front side patterning, backside patterning and etching, front side etching, and supercritical drying. The resulting front side patterns consist of a chrome mask that defines a coarse support mesh, and a silicon nitride mask for the CAT grating bars, defined by scanning-beam interference lithography (SBIL).²¹ Critical to the success of the whole process is precise alignment of the grating pattern to the $\{111\}$ planes of the $\langle 110 \rangle$ silicon surface, since the etch anisotropy between $\{111\}$ and $\{110\}$ planes of silicon in potassium hydroxide (KOH) solution is highly dependent on this parameter. The back side pattern defines a frame, and the back side etch removes the inside of the frame, stopping at the oxide layer. Front side etching in KOH results in a highly vertical etch profile all the way down to the oxide layer. A final etch in hydrofluoric acid (HF) removes the oxide and the nitride mask and produces the desired high-aspect-ratio grating bars that are freely suspended from the integrated support mesh. The sidewalls of the grating bars primarily consist of atomically flat $\{111\}$ planes. Further details are given in Ref.²⁰

Fabrication of our initial proof-of-concept prototype resulted in the following parameters (Sample A): $p = 574$ nm, $d = 10\mu\text{m}$, $\langle b \rangle = 70$ nm, and a very high grating bar aspect ratio of $d/\langle b \rangle \approx 140$. The optimum (one reflection per photon) angle of incidence for this geometry is $\alpha \approx 3^\circ$. At this value of α such a grating is expected to blaze in first order around $\lambda \approx 60$ nm. The wavelength at which $\theta_c(\lambda) \approx 3^\circ$ is $\lambda \approx 2.1$ nm. This much shorter wavelength would be blazed in 28^{th} to 29^{th} order.

In order to efficiently blaze at shorter wavelengths α needs to be reduced. This will also lead to blazing at smaller angles and therefore lower diffraction orders. Still lower diffraction orders at blaze can be achieved by going to smaller grating period. Our next step in fabrication was therefore to produce a CAT grating with

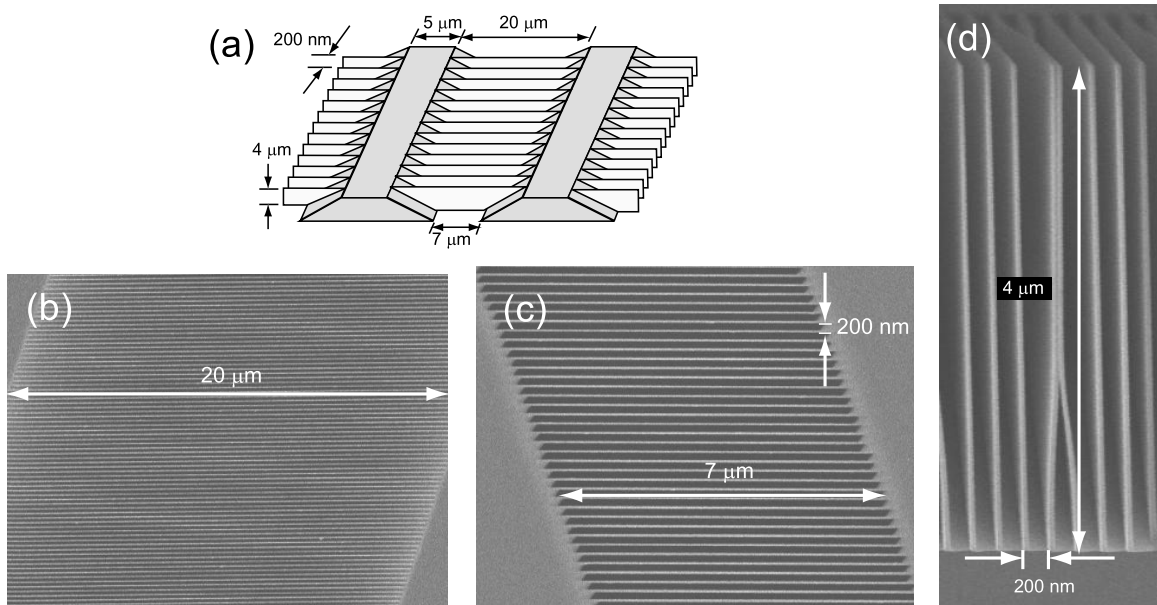


Figure 4. Fabrication results for 200 nm-period CAT gratings. (a) Schematic, showing the silicon support mesh (grey) from which the CAT grating bars are suspended. The main contribution to the diffraction efficiency comes from the area of the $7\ \mu\text{m}$ wide bottom gap between the support mesh bars. (b) Scanning electron micrograph (SEM) of a top view. (c) Bottom view (higher magnification than (b)). (d) SEM of cross section after cleaving a CAT grating along the bottom edge of a support bar, showing the high aspect ratio of the CAT grating bars. The thin grating bars frequently snap together during the destructive cleaving process.

$p = 200\ \text{nm}$. We chose SOI wafers with $4\ \mu\text{m}$ thick device layers for initial studies. If we follow the same fabrication recipe as for the $574\ \text{nm}$ -period case we end up with only about $90\ \text{nm}$ wide nitride mask lines. This is a problem, since even small misalignments between the nitride mask and the $\{111\}$ planes lead to rapid undercut during etching in KOH and eventual loss of the grating lines. In addition, we observe fast initial line thinning in KOH due to nitride mask line-edge roughness. We therefore developed an image-reversal process that gives us $140\ \text{nm}$ wide nitride lines, and improved our alignment capabilities to better than $\pm 0.05^\circ$. With these process improvements we now routinely achieve etch anisotropy ratios > 300 and $4\ \mu\text{m}$ tall and $40\ \text{nm}$ thin grating bars²² (see Sample B in Fig 4).

4. EXTREME ULTRAVIOLET AND SOFT X-RAY DIFFRACTION EFFICIENCIES

The diffraction efficiency for Sample A was measured at beam line 6.3.2 of the Advanced Light Source at the Lawrence Berkeley National Laboratory from $\lambda = 1.62$ to $50\ \text{nm}$.¹⁵ The grating was rotated by $\alpha = 2.8^\circ$ from normal incidence. Due to the slightly trapezoidal grating bar profile the sidewalls were inclined by $\sim 0.17^\circ$ from the grating normal, and the effective blaze angle was at $2 \times (2.8 + 0.17)^\circ = 5.94^\circ$ relative to the incident synchrotron beam.¹⁵

We observed the expected strong blazing, centered around a constant angle. As shown in Fig. 5, the blaze envelope started out narrow at shorter wavelengths and broadened towards longer wavelengths in accordance with our simple model. We observed up to 33^{rd} order at blaze at the shortest wavelength. The qualitative blazing behavior is in complete agreement with RCWA predictions. We normalized the measured diffraction efficiencies to the direct beam, the synchrotron ring current, and the grating open area fraction. We observed normalized diffraction efficiencies up to 46% in a single peak, and 22 – 55% within the blaze envelope at most wavelengths. This corresponds to experimental efficiencies of 65 – 80% of the RCWA predictions.¹⁵ While these efficiencies are probably close to or above record highs for diffraction gratings in this wavelength band we believe that the difference from theory is mostly due to structural defects in the gratings that we have observed in a scanning electron microscope (SEM).^{15,20} The process improvements we have employed since these measurements were

taken have greatly reduced the frequency of any SEM-detectable defects. Thus we believe that the diffraction efficiencies can still be improved.

We have very recently tested our first 200 nm-period CAT gratings with x rays in the same setup as described above. Grating parameters were similar to those shown in Fig. 4. We show raw data (unnormalized) for detector scans at a few wavelengths in Fig. 6. Similar to the case for Sample A we observe the expected strong blazing around the angle of specular reflection from the grating bar sidewalls $\approx 2 \times 2.6^\circ = 5.2^\circ$, except that due to the shorter period lower orders $|m|$ are at blaze for a given wavelength. One can also see nicely that the blazing effect diminishes as we go from 2.4 nm wavelength to 1.6 nm, since we now have moved below the wavelength where the angle of incidence ($\alpha = 2.6^\circ$) is smaller than $\theta_c(\lambda)$. At even shorter wavelengths the blazing effect is not visible anymore on a linear scale, and we observe strong transmission in the 0^{th} order, and weak $\pm 1^{st}$ orders as expected for a weak, slightly tilted phase/amplitude grating.

5. DISCUSSION, SUMMARY, AND OUTLOOK

The CAT grating design offers a new option in the design of instrumentation in the EUV and soft x-ray band. Our current fabrication effort is focused on silicon as the grating material, since its highly anisotropic etch properties in aqueous alkaline solutions provide the ability to create structures with an unsurpassed combination of high-aspect ratios and low sidewall roughness (as low as 0.2 nm). The short wavelength cutoff is therefore determined by the reflectivity of silicon as a function of incidence angle and wavelength. While shifting the cutoff to higher energies might not be necessary for Constellation-X, it would require going to smaller graze angles, which in turn demands even higher aspect ratio grating bars that are increasingly more difficult to fabricate. However, for the designs described above we do not anticipate insurmountable difficulties. We already have demonstrated aspect ratios of > 140 at 574 nm period, and we are currently working towards a value of 150 at 200 nm period (6 $\mu\text{m}/40$ nm). We also believe that it is possible to coat CAT gratings conformally with ≈ 5 nm thin metal layers via atomic layer deposition²³ to increase the reflectivity of the grating bar sidewalls and thus to extend blazing towards higher energies. As with other grazing-incidence reflectors the ability to engineer the reflecting surface offers an additional degree of freedom in the design of CAT gratings. Further potential applications are alluded to in Ref. 15.

Another area of development is the improvement of the open grating area. We have gone from 7% at 574 nm period to nominally 17.5% and 28% open area at 200 nm period through the use of thinner support mesh bars and thinner SOI device layers. Efforts are underway to prevent the loss of open area from the sloped $\{111\}$ support mesh sidewalls by preceding a shortened KOH etch step with a lattice-independent, anisotropic etch step such as deep reactive ion etching.

Some previous comparisons between x-ray telescope grating mounts juxtaposed theoretical resolution achievable in the off-plane mount and resolution for a transmission grating, with the implicit assumption that higher orders would be utilized in the off-plane case, but that only the first order could be used with the transmission grating.²⁴ With the demonstration of CAT gratings this limitation has been eliminated. We have shown that high-efficiency blazing in transmission is possible, and thus higher diffraction orders can be used in transmission to increase spectral resolution as well. Similarly, resolution-enhancing techniques such as sub-aperturing can be applied to transmission and off-plane gratings alike.

The importance of grating period for dispersion and resolution would be reduced if it is possible to blaze effectively for arbitrarily high diffraction orders (see Eq. (1)). Blazing for higher and higher orders is mainly limited by the ability to fabricate grating geometries with structural perfection down to length scales significantly smaller than the wavelengths of the diffracted light. In that regard, reliance on the atomic lattice of a single crystal as in the case of KOH etching of silicon might have an advantage over conventional etching and coating methods typically applied in the manufacture of blazed reflection gratings.

But even if a move to periods smaller than 200 nm were desired this would not present an obstacle, since we now have the demonstrated capability to interferometrically pattern large substrate areas with grating patterns down to 50 nm periods (20,000 lines/mm).²⁵

In summary, we have provided a solution to the problem of high-efficiency broadband diffraction for transmission gratings in the EUV to soft x-ray band with the introduction of the critical-angle transmission grating.

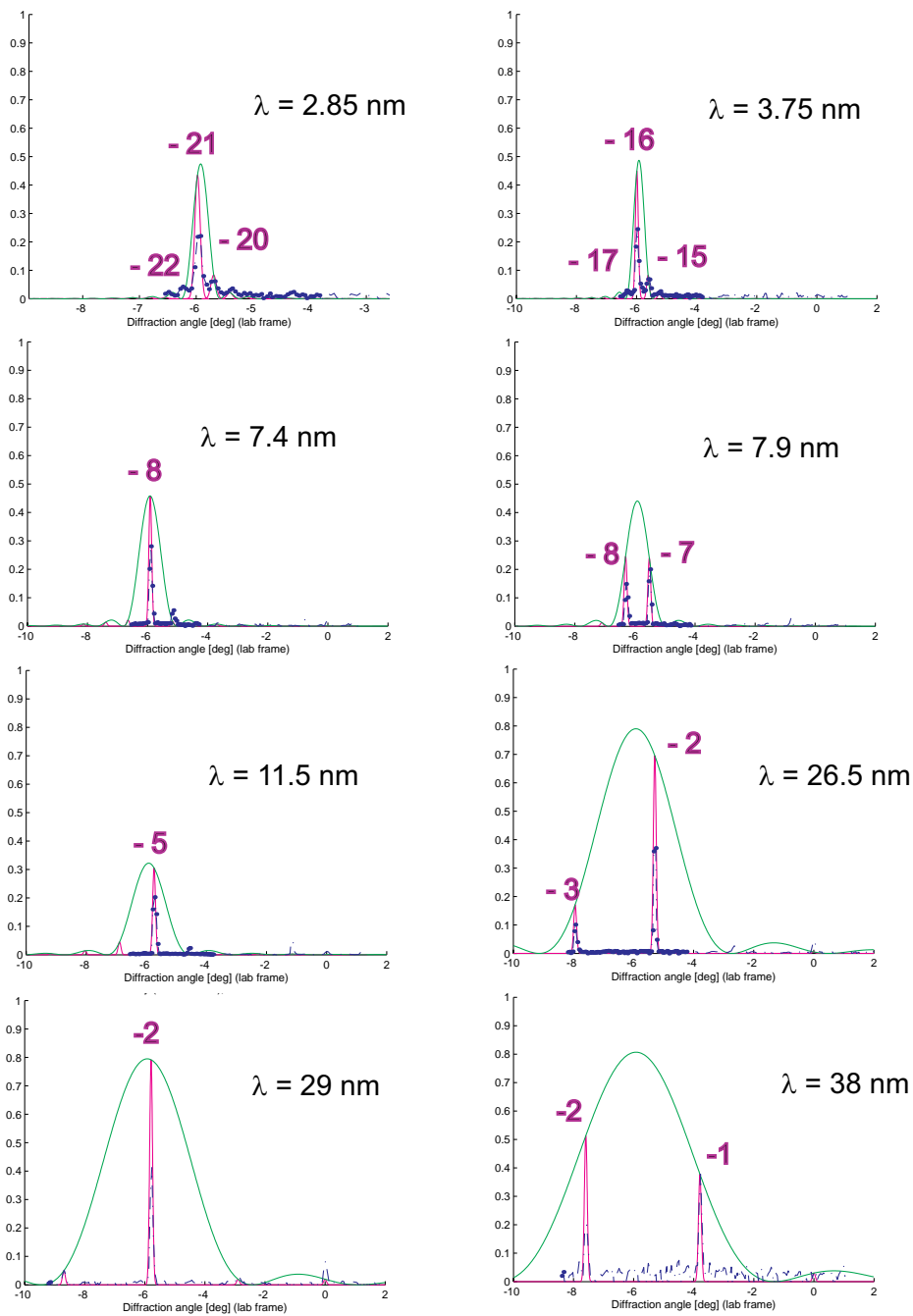


Figure 5. Normalized diffraction efficiencies from Sample A for some representative wavelengths as a function of angle from the 0^{th} order straight-through beam. The data points are the measured diffraction efficiencies, the broader peaks are the blaze envelope functions from the simple model described in Section 2.1, and the narrow peaks are the predictions from Eq. (2), broadened by the experimental detector scan line width of the direct synchrotron beam.

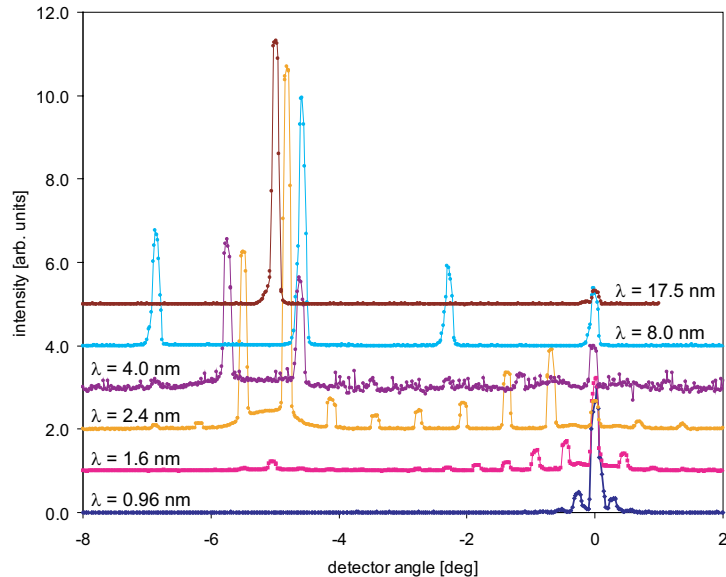


Figure 6. Detector scan data from gratings similar to Sample B ($p = 200$ nm) for some representative wavelengths as a function of angle from the 0^{th} order straight-through beam. Scans for different wavelengths are shifted for clarity. For each wavelength a separate normalization procedure needs to be applied. The blazed orders are 1, 3, 5 and 6, 7 and 8, and 12 (from 17.5 nm (top) through 1.6 nm (second from bottom)).

We have taken this approach from concept to physical demonstration and are offering a promising avenue for soft x-ray and EUV spectroscopy for astronomy and other fields.

ACKNOWLEDGMENTS

We gratefully acknowledge technical support from R. C. Fleming (Space Nanotechnology Laboratory) and J. Daley (Nanostructures Laboratory), as well as facilities support from the Microsystems Technology Laboratories (all at MIT). We also thank Eric Gullikson for his support for the x-ray measurements at the Advanced Light Source. This work was supported by NASA grants NNX07AG98G and NNX08AI62G and a Samsung Scholarship.

REFERENCES

- [1] F. B. S. Paerels and S. M. Kahn, "High-resolution x-ray spectroscopy with Chandra and XMM-Newton," *Ann. Rev. Astron. Astrophys.* **41**, 291-342 (2003).
- [2] F. D. Seward *et al.*, "Calibration and efficiency of the Einstein objective grating spectrometer," *Appl. Opt.* **21**, 2012-2021 (1982).
- [3] F. B. S. Paerels, A. C. Brinkman, A. J. F. Denboggende, P. A. J. Dekorte, and J. Dijkstra, "The EXOSAT low-energy imaging telescopes and transmission grating spectrometers - calibration and in-flight verification," *Astron. Astrophys. Suppl. Ser.* **85**, 1021-1048 (1990).
- [4] C. R. Canizares *et al.*, "The Chandra high-energy transmission grating: Design, fabrication, ground calibration, and 5 years in flight," *PASP* **117**, 1144-1171 (2005).
- [5] J. W. den Herder *et al.*, "The reflection grating spectrometer on board XMM-Newton," *Astron. Astrophys.* **365**, L7-L17 (2001).
- [6] A. E. Franke *et al.*, "Super-smooth x-ray reflection grating fabrication," *J. Vac. Sci. Technol. B* **15**, 2940-2945 (1997).
- [7] A. Rasmussen *et al.*, "Grating arrays for high-throughput soft x-ray spectrometers," *Proc. SPIE* **5168**, 248-259 (2004).

- [8] L. I. Goray, "Rigorous efficiency calculations for blazed gratings working in in- and off-plane mountings in the 5-50-Å wavelengths range," *Proc. SPIE* **5168**, 260-270 (2004).
- [9] R. K. Heilmann *et al.*, "Advances in reflection grating technology for Constellation-X," *Proc. SPIE* **5168**, 271-282 (2004).
- [10] R. L. McEntaffer *et al.*, "X-ray performance of gratings in the extreme off-plane mount," *Proc. SPIE* **5168**, 492-498 (2004).
- [11] C.-H. Chang *et al.*, "High fidelity blazed grating replication using nanoimprint lithography," *J. Vac. Sci. Technol. B* **22**, 3260 (2004).
- [12] J. F. Seely *et al.*, "Efficiency of a grazing-incidence off-plane grating in the soft-x-ray region," *Appl. Opt.* **45**, 1680-1687 (2006).
- [13] W. C. Cash Jr., "X-ray optics 2: A technique for high-resolution spectroscopy," *Appl. Opt.* **30**, 1749-1759 (1991).
- [14] W. C. Cash and A. F. Shipley, "Off-plane grating mount tolerances for Constellation-X," *Proc. SPIE* **5488**, 335-340 (2004).
- [15] R. K. Heilmann, M. Ahn, E. M. Gullikson, and M. L. Schattenburg, "Blazed high-efficiency x-ray diffraction via transmission through arrays of nanometer-scale mirrors," *Opt. Express* **16**, 8658-8669 (2008).
- [16] D. T. Attwood, *Soft X-Rays and Extreme Ultraviolet Radiation: Principles and Applications* (Cambridge University Press, 1999).
- [17] M. Born and E. Wolf, *Principles of Optics* (Cambridge University Press, 1998).
- [18] M. G. Moharam, D. A. Pommet, E. B. Grann, T. K. Gaylord, "Stable implementation of the rigorous coupled-wave analysis for surface-relief gratings - enhanced transmittance matrix approach," *J. Opt. Soc. Am. A* **12**, 1077-1086 (1995).
- [19] K. Flanagan *et al.*, "Spectrometer concept and design for x-ray astronomy using a blazed transmission grating," *Proc. SPIE* **6688**, 66880Y (2007).
- [20] M. Ahn, R. K. Heilmann, and M. L. Schattenburg, "Fabrication of ultrahigh aspect ratio freestanding gratings on silicon-on-insulator wafers," *J. Vac. Sci. Technol. B* **25**, 2593-2597 (2007).
- [21] R. K. Heilmann, C. G. Chen, P. T. Konkola, M. L. Schattenburg, "Dimensional metrology for nanometer-scale science and engineering: Towards sub-nanometer accurate encoders," *Nanotechnology* **15**, S504-S511 (2004).
- [22] M. Ahn, R. K. Heilmann, and M. L. Schattenburg, "Fabrication of 200 nm-period blazed transmission gratings on silicon-on-insulator wafers," submitted to *J. Vac. Sci. Technol. B*.
- [23] J. W. Elam, D. Routkevitch, P. P. Mardilovich, and S. M. George, "Conformal coating on ultrahigh-aspect-ratio nanopores of anodic alumina by atomic layer deposition," *Chem. Mat.* **15**, 3507-3517 (2003).
- [24] C. Lillie, W. Cash, N. Arav, J. M. Shull, and J. Linsky, "High-resolution soft x-ray spectroscopy for Constellation-X," *Proc. SPIE* **6686**, 668612 (2007).
- [25] C.-H. Chang, Y. Zhao, R. K. Heilmann, and M. L. Schattenburg, "Fabrication of 50 nm-period gratings with multilevel interference lithography," *Optics Letters*, doc ID 95394 (posted 11 June 2008, in press).